Isı Bilimi ve Tekniği Dergisi, 34, 2, 129-141, 2014
J. of Thermal Science and Technology

ISSN 1300-3615

HEAT TRANSFER ENHANCEMENT BEHIND A BACKWARD FACING STEP WITH ACTIVE FLOW CONTROL

Sertac CADIRCI* and Hasan GUNES**
Department of Mechanical Engineering, Istanbul Technical University
34437 Gumussuyu, Istanbul,
*cadircis@itu.edu.tr, **guneshasa@itu.edu.tr

(Geliş Tarihi: 22.10.2013, Kabul Tarihi: 10.01.2014)

Abstract: In this study we investigate simulate the heat transfer enhancement behind a backward facing step with active flow control. The numerical simulations are carried out by a finite volume based laminar, incompressible, unsteady flow solver (ANSYS-Fluent) in a two-dimensional computational domain with Cartesian cells including a moving zone to mimic the periodic motion of the actuator plate. The active flow control device used is a Jet and Vortex Actuator (JaVA) that is shown previously to delay or prevent flow separation. JaVA in its simple form is a rectangular cavity containing an asymmetrically located plate on its opening which moves in horizontal direction with a certain amplitude and frequency. Depending on the motion of the plate, fluid is either ejected out of the cavity or sucked into the cavity. The jet or vortex ejected downstream of the backward facing step transport momentum to the base flow, increases the mixing and thus enhancing heat transfer. Keeping the amplitude and the plate width constant for all cases, it is observed that with increasing frequency (jet-Reynolds number), the traveling vortical structures form downstream of the channel. These vortical structures significantly increase the rate of heat transfer due to better mixing. It is reported that the forming vortical structures in channel is the main mechanism for the increase of heat transfer. It is found that as the incoming flow Reynolds number increases, the extent of the traveling vortical structures moves far downstream distances and the Nu values are much higher compared to the non-actuated base flow.
Keywords: Active Flow Control, Jet and Vortex Actuator (JaVA), Backward Facing Step (BFS) Flow, Heat Transfer Enhancement, Computational Fluid Dynamics (CFD).

AKTİF AKIŞ KONTROLÜ İLE TERS BASAMAK ARDINDAKİ ISI GEÇİŞİNİN İYİLEŞTİRİLMESİ

Özet: Bu çalışmada ters basamak ardındaki ısı geçişinin aktif akış kontrolü ile iyileştirilmesi sayısal olarak incelenmiştir. Sayısal modellemeler sonlu-hacimler tabanlı laminer, sıkıştırılamaz, daimi olmayan akış çözücü (ANSYS-Fluent) ile kartezyen elemanlardan oluşan ve aktüatör plakasının periyodik hareketini temsil eden hareketli bir bölge bulunduran iki boyutlu bir çözüm ağında yapılmıştır. Aktif akış kontrol düzeneği olarak kullanılan Jet ve Vorteks Aktüatörünün (JaVA) akış ayrılmasını geciktirdiği veya engellediği daha önceki çalışmalarda gösterilmiştir. JaVA gövdesi dikdörtgen kesitli bir kavitedir ve açık olan üst kısmında asimetrik olarak yerleştirilmiş bir levha belirli bir genlik ve frekans ile yatay doğrultuda hareket etmektedir. Levhanın hareketine bağlı olarak akışkan kavite içerisine emilmekte veya kaviteden dışarı enjekte edilmektedir. Oluşan jet veya vorteks akışları, ters basamak aşağıakım bölgesinde, kanal akışına momentum transportu sağlamakta ve aynı zamanda karışımı arttırarak ısı geçişini iyileştirmektedir. Genlik ve levha genişliği sabit tutularak, artan frekans ile (jet-Reynolds sayısı) ters basamak aşağıakım bölgesinde ilerleyen vorteks yapılarının oluşumu gözlemlenmiştir. Bu yapılar daha iyi bir karışım sağlayarak ısı transferini iyileştirmektedirler. Kanal içerisinde oluşan bu vorteks yapıları ısı geçişinin iyileştirilmesindeki ana mekanizmadır. Kanal akışının Reynolds sayısının artması ile JaVA-kaynaklı vorteks yapıları aşağıakım bölgesinde daha da ileriye taşınmakta ve Nusselt sayısı aktüasyon olmayan duruma göre oldukça yükselmektedir.
Anahtar Kelimeler: Aktif Akış Kontrolü, Jet ve Vorteks Aktüatörü (JaVA), Ters Basamak Akışı, Isı Geçişi, Hesaplamalı Akışkanlar Dinamiği (HAD).

SYMBOLS

Roman Characters

a	actuator plate amplitude [=1.0 mm]
b	step height [=28.1 mm]
C_p	specific heat [J/kgK]
D_H	hydraulic diameter at inlet [= $2b$]
f	operating frequency of the actuator [Hz]

h convection coefficient [W/m^{2}K]
k_f thermal conductivity of the fluid [=0.6 W/mK]
Nu Nusselt number [$=q_w D_H/(\Delta T)k_f$]
p pressure [N/m^2]
q_w wall heat flux [W/m^2]
Q flowrate [mm^3/s]
$\mathrm{Re_J}$ Reynolds number of the jet flow [$= 4awf/\nu$]
Re Reynolds number of the main flow [$= u_m D_H/\nu$]
$\mathrm{S_a}$ scaled amplitude [$= 2\pi a/w$]
t time [s]
T temperature [K]
u streamwise velocity component [mm/s]
u_m average velocity of the main flow at inlet [mm/s]
U_{max} maximum velocity of the main flow [mm/s]
V velocity vector [mm/s]
V_J mean jet speed [mm/s]
V_P speed of the plate [mm/s]
w actuator plate width [=25 mm]
w_n narrow slot [=0.3 mm]
w_w wide slot [=2.5 mm]
x x-coordinate (vertical axis)
y y-coordinate (horizontal axis)

Greek Symbols

ε relative error
θ normalized temperature [$=(T_f-T_{wall})/(T_h-T_c)$]
μ fluid viscosity [$=10^{-3}$ kg/ms]
ν kinematic viscosity of the fluid [m^2/s]
ρ fluid density [=1000 kg/m^3]

INTRODUCTION

Active flow control is an attractive topic in the fluid mechanics to which many researchers devote their attention in the last two decades. One of the active flow control systems is the zero-net-mass flux (ZNMF) actuation system which does not require any external fluid to operate and any internal fluid supply lines. The advantage of ZNMF actuators is that they have a wide range of flow control applications due to their potential use in separation control, flow mixing, heat transfer enhancement etc. ZNMF actuators can be different in their design and driving system. A typical ZNMF actuator consists of a driver which generates the volume displacement, a cavity where fluid is periodically sucked and ejected and a slot or orifice where fluid is expelled in forms of a jet or vortex. The driver system of a ZNMF actuator can have a mechanic, piezoelectric or electro-dynamic transduction (Cattafesta, 2009).

ZNMF actuators can be successfully applied to prevent/delay boundary layer separation at high Reynolds numbers (Seifert and Pack, 1998), for instance vortex generators can be used to control boundary layer separation during takeoff and landing of aircrafts (Johnston and Nishi, 1990). One of the typical and promising ZNMF devices for active flow control is the Jet and Vortex Actuator (JaVA). JaVA tested in quiescent air can produce jets of different orientation or vortex flows as reported in detail in (Lachowicz *et al*., 1999a-b).

Another JaVA-device similar to that device reported by (Lachowicz *et al*., 1999) is a mechanically driven active flow control device which is investigated experimentally in quiescent water by (Gunes *et al*., 2008) and (Cadirci *et al*., 2012) to show the effect of several actuation parameters on the JaVA-induced flows. Flow visualizations and Particle Image Velocimetry (PIV) measurements carried out in water revealed that the main JaVA-induced flow regimes include jets to different directions and chaotic vortex flows. The type and strength of these JaVA-induced flow regimes are significantly influenced by the actuation parameters such as the frequency, amplitude and slot width of the cavity.

JaVA mounted on a flat plate is investigated by flow visualizations and Particle Image Velocimetry (PIV) measurements to reveal the interaction of JaVA-induced flow regimes with the laminar boundary layer (Cadirci, 2011). In addition to experimental studies, JaVA-induced flow regimes in a laminar boundary layer are also investigated numerically by solving unsteady incompressible Navier-Stokes equations by imposing user-specified boundary conditions (Cadirci *et al*., 2010 and 2013). Both experimental and numerical investigations of JaVA under cross-flow conditions revealed that the boundary layer profiles gain additional momentum flux at various actuation frequencies and thus get a "fuller" shape compared to the non-actuated case (base-flow). Specifically, it is shown that JaVA leads to a certain decrease in the displacement thicknesses and shape factors as well as an increase in the friction coefficient (Cadirci *et al*., 2013).

Several active flow control strategies are utilized to control backward-facing step (BFS) flows. Pulsing inlet velocity and alternatively local oscillating jets implemented on the step's vertical wall are examples for active flow control behind a BFS where the effect of open-loop and close-loop on the recirculation region is tested (Creuse *et al*., 2009). An analytical approach is developed for closed-loop separation control in steady and unsteady channel flows with the aim to reduce the recirculation length behind the BFS (Alam *et al*., 2006). Channel flow behind a BFS is studied experimentally and it is observed that the blowing and suction are able to reduce the length of the separation zone compared to that of without control (Uruba *et al*., 2007). A numerical study carried out to investigate the frequency effect of a zero-mass-flux on a generic separated flow over a smooth ramp showed that the separation length can be reduced significantly (Dandois *et al*., 2007).

There are numerous studies where the heat transfer enhancement behind a BFS is investigated. For instance the use of nanofluids can enhance the heat transfer in separated flows encountered in a BFS. Laminar forced convection flow over a BFS using nanofluids has been investigated numerically by (Al-aswadi *et al*., 2010). Various types of nanoparticles dispersed in a base fluid at low Reynolds numbers affect the velocity profiles extracted at different locations downstream of the

channel. Another numerical study investigates the application of nanofluids for heat transfer enhancement of separated flows encountered in a BFS (Nada, 2008). The aim of the study is to increase the averaged Nusselt number with the volume fraction of nanoparticles. The Nusselt number distribution along the top and bottom walls of the channel using nanoparticles has increased considerably compared to the base-flow without nanoparticles.

In this study, active control of flow behind a BFS in a narrow channel is investigated numerically using an oscillatory, ZNMF system where the principle of the control strategy is similar to those mentioned in (Gunes *et al*., 2008; Cadirci *et al*., 2010, 2012, 2013). The aim of the current study is to prevent flow separation behind a BFS and enhance mixing downstream of BFS through JaVA-induced flow regimes. As a result it is aimed to increase the rate of heat transfer downstream of the channel thus the Nusselt numbers along top and bottom walls of the channel are compared for actuator on- and off cases.

COMPUTATIONAL DOMAIN AND BOUNDARY CONDITIONS FOR JaVA-BFS

Jet and Vortex Actuator (JaVA)

The main part of JaVA is a two-dimensional rectangular cavity with an actuator plate which is moving back and forth like a piston. The actuator plate is mounted asymmetrically on the opening of the cavity such that there are one narrow (w_n) and one wide gap (w_w) between the actuator plate and the edges of the cavity. The main parameters governing JaVA-induced flow regimes are the actuator plate's width (w), the amplitude (a) and the operating frequency (f). The mean position of the actuator plate with respect to the JaVA-cavity is fixed for all cases, namely it is flush-mounted with BFS. For the current investigations, the plate has a width of w = 25 mm, and the actuator amplitude is a = 1.0 mm. The operating frequencies vary between 1 and 3 Hz.

Non-dimensional numbers such as the scaled amplitude ($S_a = 2\pi a/w$) and the jet Reynolds number (Re_J) can be derived from those parameters to characterize JaVA-induced flow types. The scaled amplitude only changes with the amplitude as we kept the plate width constant at 25 mm. The mean jet velocity of the JaVA-induced flows can be defined by integrating time-averaged jet velocity over the half period as given in Eq. (1). The integration should be over half a cycle to predict the jet velocity of a single phase since one single period consists of blowing (ejection) and suction phases. The volumetric flow rate Q is the fluid displacement during the motion of the actuator plate through the wide gap.

$$V_J = \frac{Q}{w_w} = \frac{1}{w_w}\left[\frac{2}{T}\int_0^{T/2} v_j(t)\,dt\right] = \frac{4awf}{w_w} \qquad (1)$$

The jet Reynolds number (Re_J) given in Eq. (2) is derived from the volumetric flow-rate over half cycle assuming that the displaced volume of fluid is equal to the product of the unit depth with the amplitude and the actuator plate width (Cadirci, 2011). As we keep the amplitude and actuator plate width constant, the jet Reynolds number will only vary with the frequency.

$$\mathrm{Re}_J = \frac{\rho V_J w_w}{\mu} = \frac{4awf}{\nu} \qquad (2)$$

The operating principle is based on the motion of the plate (which is the step height in BFS flow). When the actuator plate moves into the cavity to eject a jet or vortices out of the wide gap into the BFS, it is called blowing. When the plate moves out of the cavity, the fluid is sucked into the cavity and it is called suction. These jet and/or vortices energize the channel flow and help mixing of the flow downstream of BFS. JaVA can be used to control the flow and re-attachment and enhance heat transfer characteristics.

Computational Domain and Boundary Conditions

Figure 1 shows the sketch of the problem geometry and the boundary conditions. The height of the inflow section is equal to the step height. The step height is equal to the sum of the actuator plate width (w = 25 mm), the wide gap (w_w = 2.5 mm) and two narrow spacing (0.6 mm), thus it is 28.1 mm and the height of the inflow section is also b = 28.1 mm. The leading edge of the BFS is the origin of the computational domain. The lengths upstream and downstream of the origin (step) are 4b and 36b respectively. It is believed that downstream length is sufficient to apply pressure outlet boundary conditions as well as to investigate the effect of the actuator downstream of the BFS.

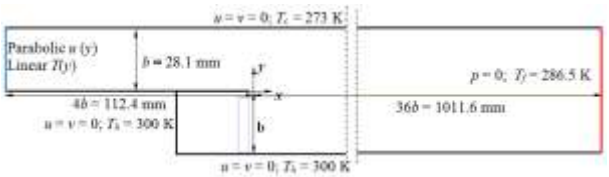

Figure 1. Sketch of the computational geometry and boundary conditions for JaVA-BFS.

The computational domain consists of Cartesian cells and the grid is refined near the JaVA-cavity and wide gap from which the jet or vortices are ejected. The motion of the actuator plate is generated by a moving zone between two sliding interfaces along the channel. To obtain reliable results, the computational domain is clustered in close vicinity of the actuator and along the channel walls. A typical two-dimensional grid consists of nearly 167000 Cartesian cells.

JaVA-induced flows are time-dependent thus long transient solutions are needed to obtain reliable steady-state results in the flow domain. JaVA-induced flow fields are obtained by time-accurate flow solutions where the time step per iteration is kept constant at Δt =

0.003125 (1/320) seconds and the solution is integrated for a minimum of 1000 seconds (c.a. 3-4 days). Further 20 periods that correspond to 200 instantaneous snapshots have been computed to obtain the time-averaged flow and temperature fields and extract velocity and temperature profiles. The detail of the computational domain is demonstrated in Fig. 2.

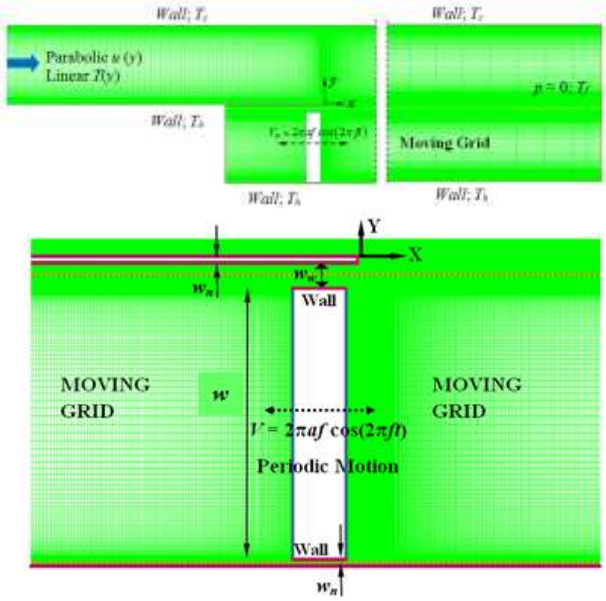

Figure 2. Detail of the computational domain near BFS/JaVA.

The computations have been carried out by a finite-volume-based laminar, incompressible, unsteady Navier-Stokes solver using commercially available software (ANSYS-Fluent). The continuity (Eq.3), momentum (Eq.4) and energy equations (Eq.5) are solved by the PISO-algorithm where for pressure and energy equation second-order and for momentum equation third-order discretization schemes are used, respectively. Appropriate underrelaxation factors have been selected to accelerate the convergence.

$$\nabla \cdot \mathbf{V} = 0 \tag{3}$$

$$\rho\left[\frac{\partial \mathbf{V}}{\partial t} + (\mathbf{V}\cdot\nabla)\mathbf{V}\right] = -\nabla p + \rho g + \mu\nabla^2\mathbf{V} \tag{4}$$

$$\rho C_p \frac{DT}{Dt} = \frac{Dp}{Dt} + \nabla\cdot\left(k_f \nabla T\right) + \Phi \tag{5}$$

The inlet of the channel is prescribed with velocity inlet condition. The velocity profile of the incoming flow given in Eq. (6) is determined by a second-order polynomial approximation to Blasius solution using no-slip boundary conditions. The inlet boundary condition is defined as a user-defined-function (UDF) where b is the height of the inflow section (28.1 mm), U_{max} is the maximum velocity and y is the coordinate in vertical direction as shown in Fig. 2.

$$u(y) = -4U_{\max}\left[\left(\frac{y}{b}\right)^2 - \left(\frac{y}{b}\right)\right] \tag{6}$$

The averaged inlet velocity of the incoming flow in Eq. (7) is determined by integrating Eq. (6) for unit depth. Using this average velocity, the Reynolds number of the incoming flow in Eq. (8) can be calculated. It should be mentioned that the hydraulic diameter of the two-dimensional channel is taken twice of the inlet section's height. To maintain laminar channel flow, Reynolds numbers at the inlet are restricted to 200 and 400. The pressure outlet boundary condition is employed at the BFS channel exit.

$$u_m = \frac{1}{b}\int_0^b u(y)\,dy = \frac{2U_{\max}}{3} \tag{7}$$

$$\mathrm{Re} = \frac{\rho u_m D_H}{\mu} = \frac{(4/3)U_{\max} b}{\nu} \tag{8}$$

The thermal boundary condition at the inlet is a linear function. The upper wall of the channel has a temperature T_c = 273 K and the bottom wall of the channel including the walls surrounding the JaVA cavity and the actuator plate's edges have a higher temperature T_h = 300 K. A linear user-specified function is proposed that satisfies the thermal boundary conditions at the inlet and it is given in Eq. (9). The temperature of the fluid at the exit (T_f = 286.5 K) is assumed to be the average of the top and bottom wall temperatures since the flow is hydraulically and thermally fully-developed near the exit.

$$T(y) = T_h\left(1 - \frac{y}{b}\right) + T_c\frac{y}{b} \tag{9}$$

The Nusselt number in Eq.(10) is obtained from the total heat flux along the top and bottom walls where the hydraulic diameter is taken D_H = 2b. The convection coefficient is expressed in terms of the total heat fluxes along the walls. Thermal conductivity of the fluid (k_f) is constant.

$$\mathrm{Nu} = \frac{hD_H}{k_f} = \frac{2bq_w}{\left(T_{wall} - T_f\right)k_f} \tag{10}$$

The actuator plate which is initially located exactly 1 mm behind the top of the cavity opening moves in horizontal direction with a velocity depending on the frequency and amplitude. The amplitude of the actuator (a) is taken 1 mm so that the actuator plate reaches top of the cavity opening. The horizontal edges of the actuator plate are walls with no-slip condition and the vertical edges are prescribed with periodic velocity boundary condition. The motion of the actuator plate is generated by the periodic motion which is defined as a sinusoidal function given in Eq. (11):

$$V_P = 2\pi af\cos\left(2\pi ft\right) \tag{11}$$

NUMERICAL VALIDATIONS

The numerical results given in (Nada, 2008) are used to test the reliability of our numerical results. First the BFS geometry in (Nada, 2008) with the same dimensions and boundary conditions has been created. The coarse and fine meshes tested in the validation include 45000 and 180000 elements, respectively. As Fig. 3a indicates, there is no change between the solutions obtained from the coarse and fine meshes for the base-flow case (f=0). Additionally, our numerical results in Fig.3a and 3b obtained for two Reynolds numbers agree well with the numerical results given in (Nada, 2008).

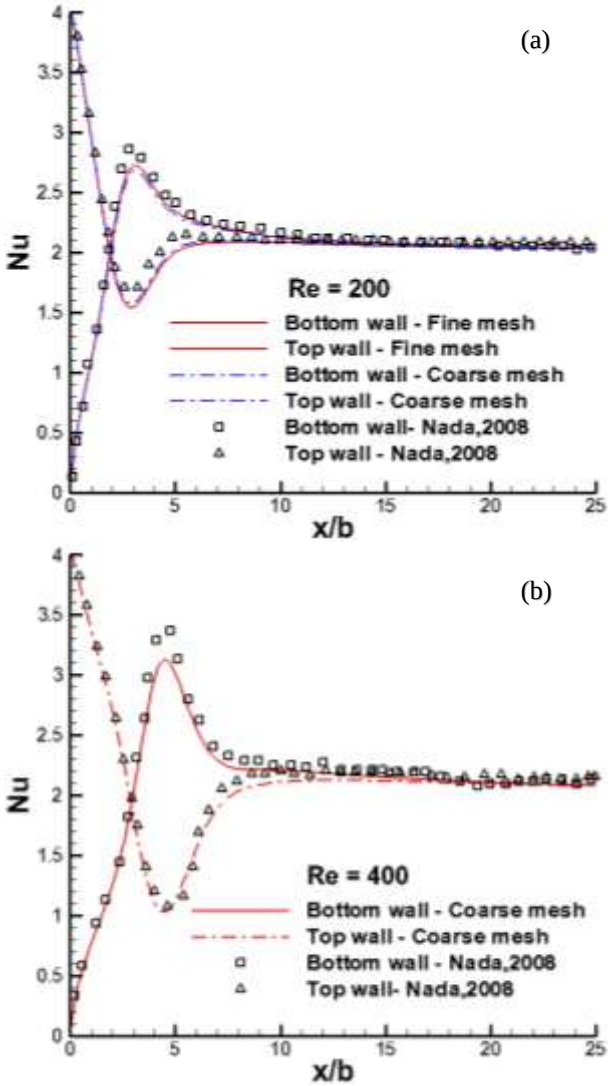

Figure 3. Comparison of the Nusselt number distributions along the channel top and bottom walls obtained from current simulations via identical BFS geometry and (Nada, 2008): (a) Re = 200 (b) Re = 400.

In Fig. 3, the maximum relative errors between (Nada, 2008) and current simulations (using identical BFS geometry) for Re = 200 are approximately $\varepsilon_{top} = \varepsilon_{bottom} =$ 5 % at around x/b = 3 and for Re = 400 they are approximately $\varepsilon_{top} = \varepsilon_{bottom} = 4$ % at around x/b = 5.

On the other hand, Fig. 4 shows the numerical results for the base-flow given in (Nada, 2008) and our simulations for the base-flow (actuator-off) obtained from the computational domain possessing JaVA (see Fig. 1). While small differences due to the step height incorporating JaVA geometry are observable, both results agree with each other for both Reynolds numbers for actuator-off condition. We also mention that the flow characteristics are even closer for the two cases.

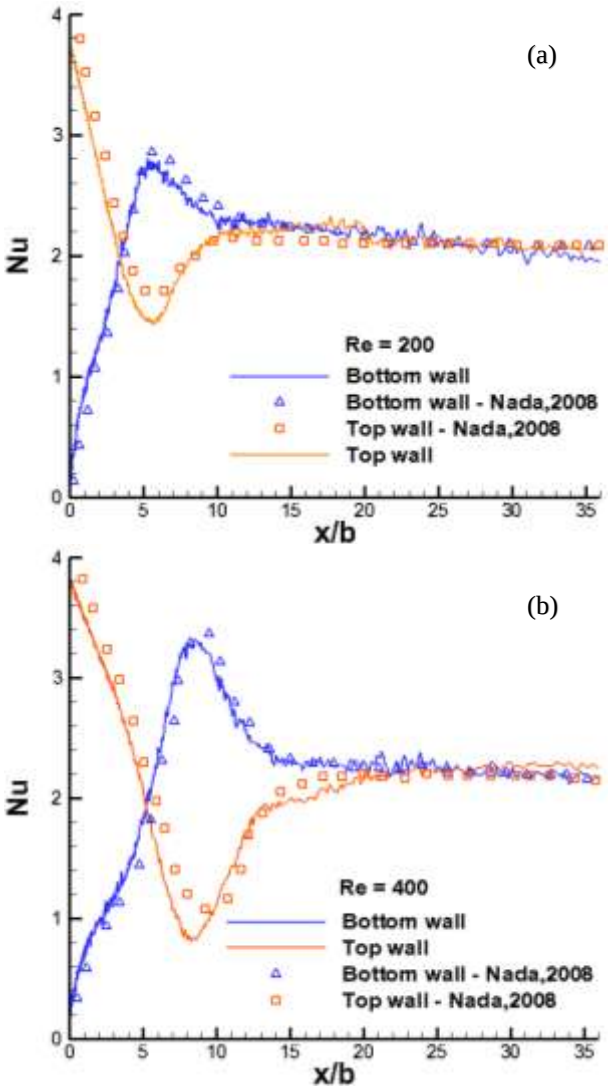

Figure 4. Comparison of the Nusselt number distributions along the channel top and bottom walls obtained from current simulations via JaVA-BFS geometry and (Nada, 2008): (a) Re = 200 (b) Re = 400.

In Fig. 4, the maximum relative errors between (Nada, 2008) and current simulations via JaVA-BFS geometry for Re = 200 are ε_{top} = 10 % and ε_{bottom} = 3 % at around x/b = 5 and for Re = 400 they are ε_{top} = 15 % and ε_{bottom} = 2 % at around x/b = 8. The maximum relative errors in the Nusselt numbers along the top walls are much higher compared to maximum relative errors in the Nusselt numbers along bottom walls because in this case the computational domains are not fully identical as in Fig.3.

JaVA-BFS RESULTS

Figure 5 indicates the effect of active flow control on time-averaged flow fields past a backward-facing-step (BFS) at several frequencies for Re = 200. In the base flow without actuation (f = 0), flow separation is observed behind the backward facing step and the dimensionless reattachment length reaches approximately $x_r = x/b = 5$ in agreement with (Nada, 2008). When the actuator operates at a frequency of 1 Hz, (which corresponds to jet Reynolds number, Re_J = 100) the jet emerging from the wide gap significantly changes the base flow characteristics and as a result the recirculation zone on the bottom wall completely disappears. On the other hand, a new larger recirculation zone forms on the upper wall. If the frequency is increased to 2 Hz (Re_J = 100), the counter-rotating vortices are formed travelling along the channel. At Re_J = 200, the jet and vortex actuator is capable of completely changing the characteristics of the downstream flow thus the channel flow downstream of JaVA now features many vortices as shown up to x/b = 12. Specifically, starting from x/b = 12 vortices begin to die out slowly till the channel outlet where the flow is almost unidirectional. A similar flow field with stronger vortices is obtained when the frequency is raised to 3 Hz (Re_J = 300), the vortices dominating the channel flow begin to die out slowly after x/b = 12 as in the previous case (Re_J = 200). It can be concluded that actuation frequency of 2 Hz is sufficient for a good mixing in the channel at Re = 200 (incoming flow Reynolds number).

Figure 6 shows time-averaged isotherms for various actuating frequencies for the incoming flow Reynolds number, Re = 200. The base-flow (f = 0) denotes the *actuation-off* case where the Nusselt number distributions along the top and bottom walls are shown in Fig. 4a. Considering the thermal boundary conditions of the base flow field, heat is transferred from the hotter bottom surface to the cooler upper surface. As Fig. 4a and isotherms in Fig. 6 indicate, the heat transfer is mainly with conduction for downstream distance $x/b > 8$ as the temperature gradually increases from the upper wall to the bottom wall linearly. However, this linear distribution is completely lost for the actuating cases. For jet Reynolds numbers, Re_J = 200 and Re_J = 300, the large temperature gradients occur at the close vicinity of the top and bottom walls, while the temperature across the channel is mostly kept at a mean value. The steep temperature gradients near walls lead to an enhanced heat transfer through an effective mixing in the channel.

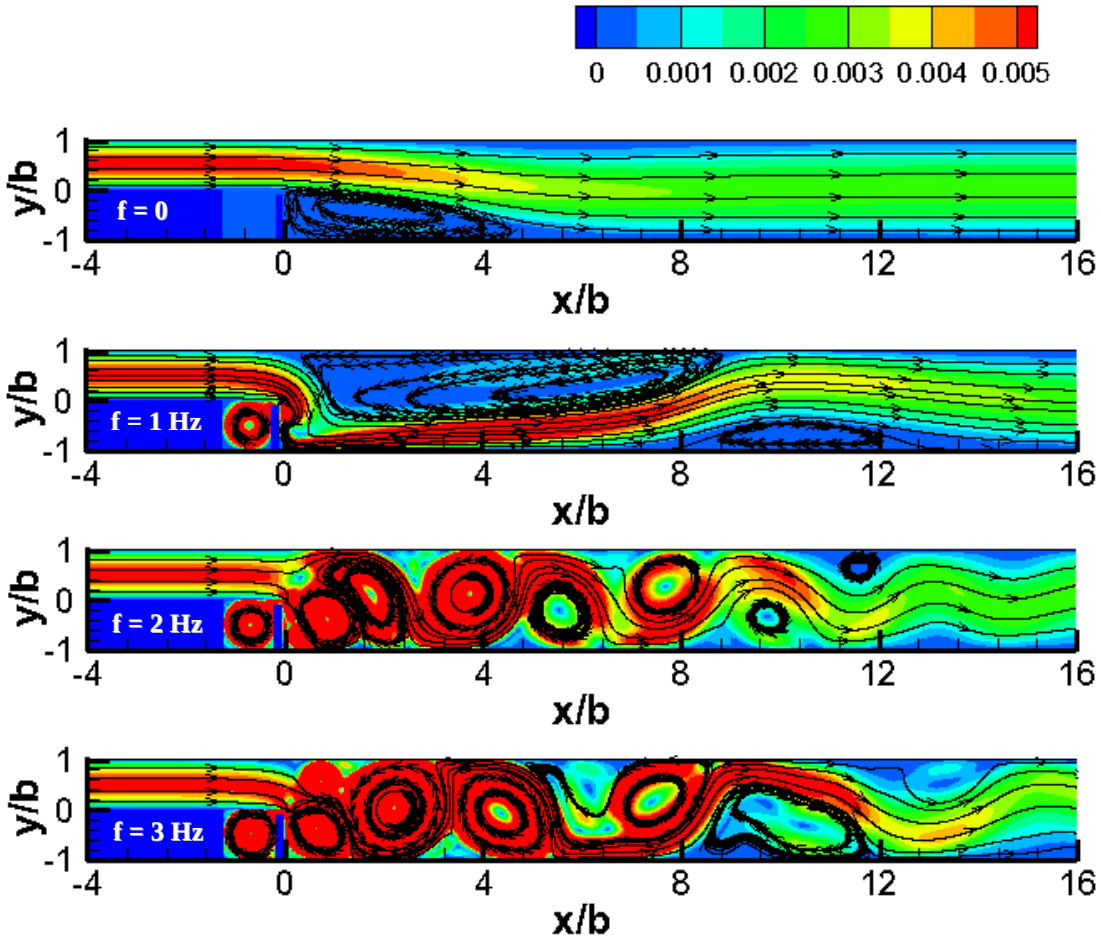

Figure 5. Time-averaged streamlines for various actuating frequencies. Colors denote the magnitude of velocity [m/s], Re = 200.

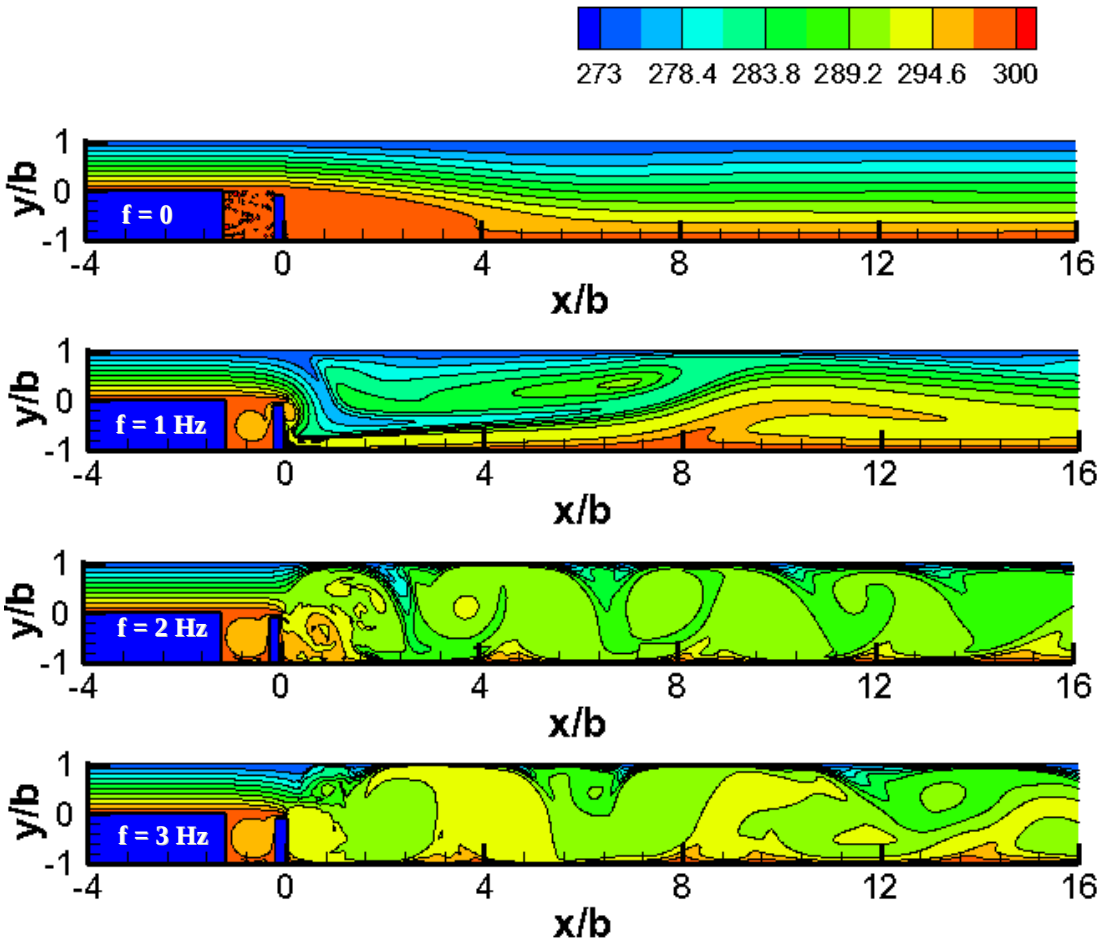

Figure 6. Time-averaged isotherms for various actuating frequencies. Colors denote the temperature [K], Re = 200.

Figure 7 shows the comparison of time-averaged channel velocity profiles for several downstream stations x/b = 4, 12, 18 and 24 at various actuation frequencies. The velocity profiles in close vicinity of the JaVA (i.e., horizontally moving step) at x/b = 4 represent significant backflows at frequencies 2 and 3 Hz, as we encounter the strongest JaVA-induced vortical flows in the vicinity of the BFS. At x/b = 12 for instance, the velocity profile of the base-flow is already fully developed and has a parabolic shape. When an actuation is applied at 2 and 3 Hz, fuller velocity profiles are achieved on the bottom wall of the channel that can resist flow separation; however at 1 Hz, a secondary vortex on the bottom wall exists at x/b = 12 so that the velocity profile features a backflow (see also Fig. 5). At another downstream station x/b = 18, all the velocity profiles possess a parabolic shape. With increasing frequency the velocity profiles at the bottom wall gain a fuller shape compared to the velocity profile of the base flow. However, near the exit of the channel, there are only minor changes in the velocity profiles as the downstream station x/b = 24 is far enough to cease the effect of actuation.

Figure 8 shows time-averaged temperature profiles at various downstream stations for Re = 200. As mentioned earlier, a user-specified linear temperature profile is prescribed at the channel inlet. In the fully-developed flow region of the base flow, the temperature profile is linear as expected. The JaVA highly increases the heat transfer from the fluid to the channel walls as reflected in the steeper temperature gradients near walls as shown in Fig. 8. Since the heat flux is linearly dependent on the temperature gradient on the walls, with increasing temperature gradient the heat flux also increases. Specifically at a downstream station in the vicinity of the actuator (x/b = 4), the temperature gradients at f = 2 Hz and 3 Hz are so high that we see a sudden jump in the heat flux (or Nusselt number) value as shown in Fig. 13. At further downstream stations such as x/b = 12, 18 and 24; the steepness of the temperature gradients reduce compared to the JaVa vicinity, but still the heat transfer rates are as high as an order of magnitude compared to the actuation-off case.

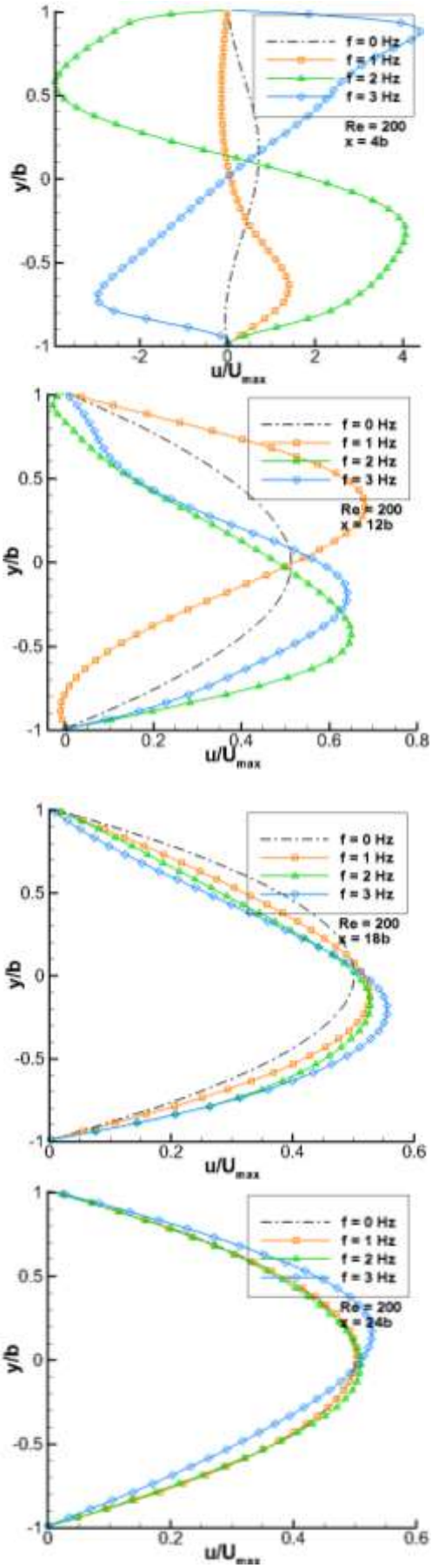

Figure 7. Streamwise velocity profiles across various channel locations, Re = 200.

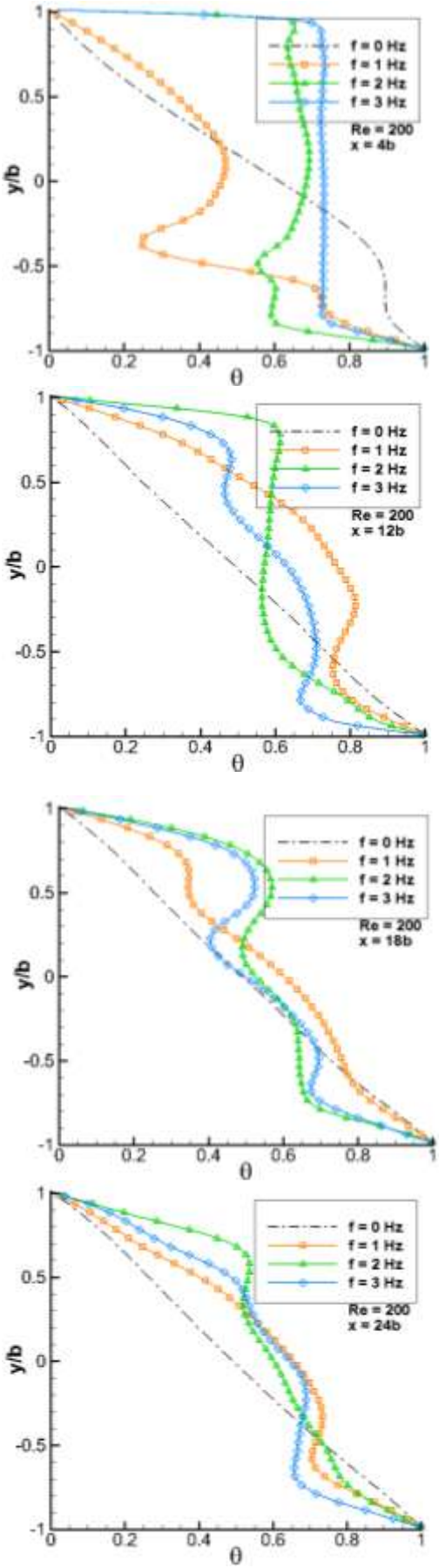

Figure 8. Streamwise temperature profiles across various channel locations, Re = 200.

Figure 9 demonstrates the time-averaged streamlines for various actuating frequencies for Re = 400. At Re = 400, the incoming flow rate (maximum inlet velocity) is twice as high compared to Re = 200. For this case, the dimensionless reattachment length in the base-flow (f = 0) is approximately $x_r = x/b = 8$ as found in (Nada, 2008). At the frequency 1 Hz, the recirculation zone on the bottom has been restricted to $x_r = x/b = 1$ but two new vortical structures occur on the top wall which are smaller in size compared to the large separation zone on the top wall at 1 Hz for Re = 200. At the frequency 2 Hz, counter-rotating vortices occur in the channel and these vortices travel downstream till x/b = 12 as observed similarly in the case Re = 200. For 3 Hz, on the other hand, vortices travel larger distances downstream before they start to die out slowly after x/b = 16. The ratio of the jet Reynolds number to incoming flow Reynolds number (Re_j/Re) is found an important parameter to characterize the extent of the vortical structures in the channel. For Re = 400, we have a higher incoming flow speed carrying the vortical structures to further downstream locations than in the case of Re = 200.

Figure 10 indicates the time-averaged isotherms for various actuating frequencies for the incoming flow Reynolds number, Re = 400. The temperature distribution is quite similar to that of the previous case (Re = 200) for actuation frequencies f = 2 Hz and 3 Hz. It is seen that with higher actuation frequency, the vortical structures become stronger and they move larger distances downstream of the channel. The temperature gradients are steeper in the top and bottom walls. It is also seen in Fig. 10 that almost uniform temperatures can be observed in the most part of the channel cross-section for f = 2 Hz and 3 Hz.

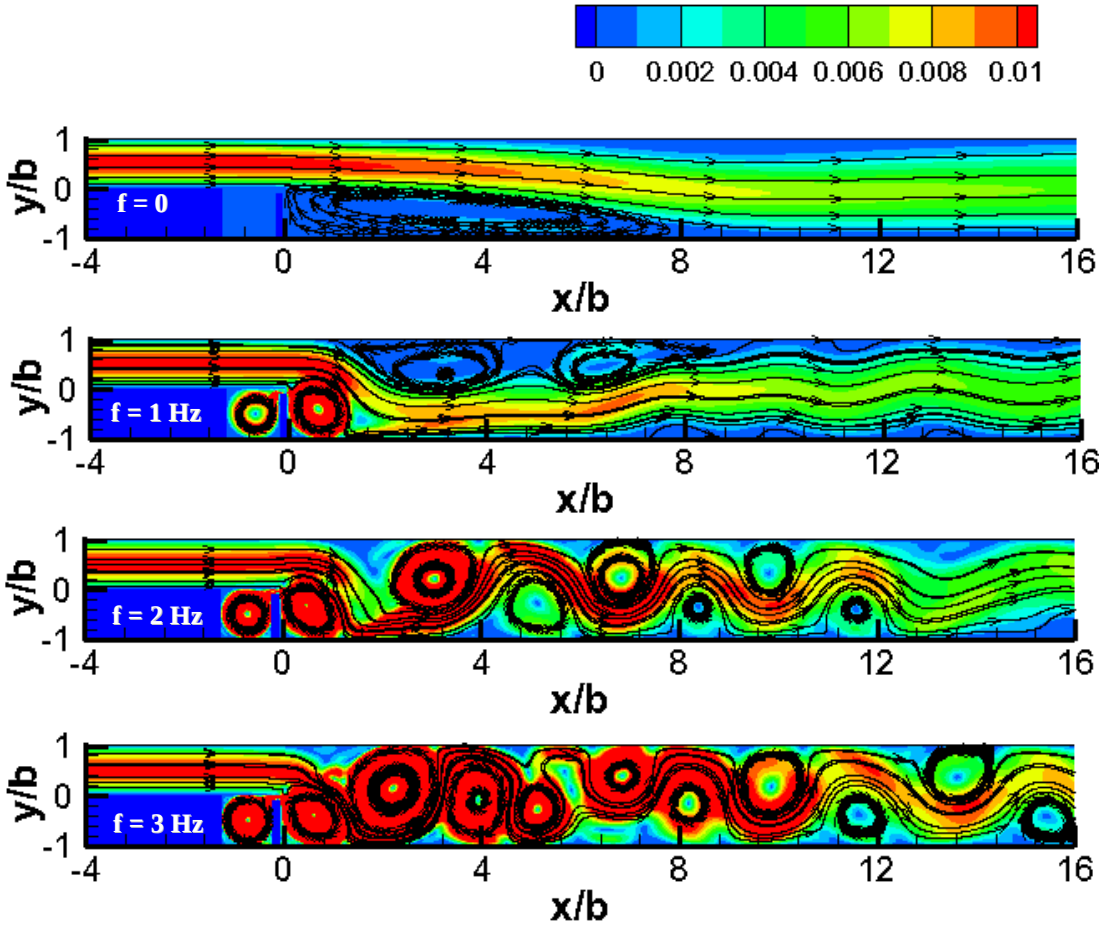

Figure 9. Time-averaged streamlines for various actuating frequencies. Colors denote the magnitude of velocity [m/s], Re = 400.

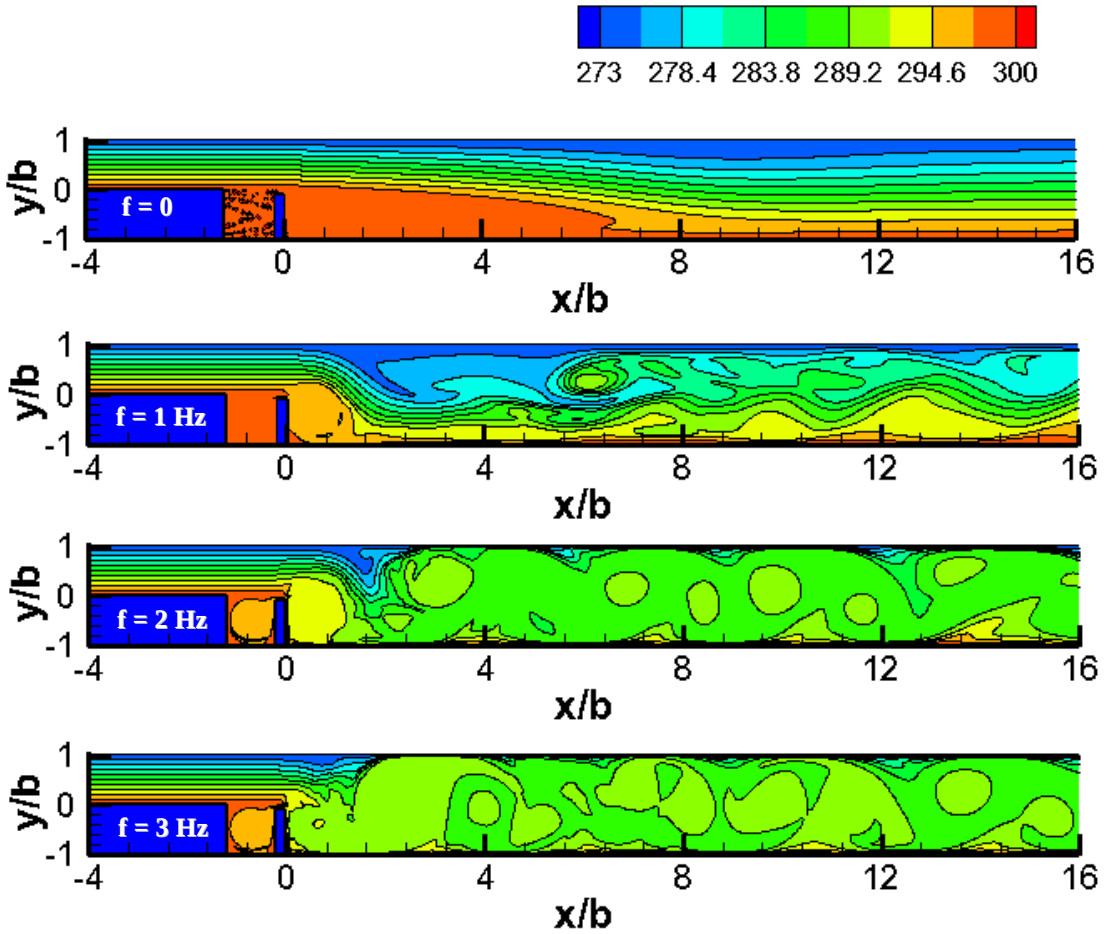

Figure 10. Time-averaged isotherms for various actuating frequencies. Colors denote the temperature [K], Re = 400.

Figure 11 displays the comparison of time-averaged channel velocity profiles for several downstream stations x/b = 4, 12, 18 and 24 at various actuation frequencies. In the vicinity of JaVA, the flow separation occurs at frequencies 2 and 3 Hz at the locations x/b = 4 and but even 12. Downstream of JaVA at the location x/b = 18 all the profiles gain a smoother parabolic shape as a result of diminished vortex pairs in the flow fields. Near the exit (x/b = 24) there are only minor changes in the velocity profiles except the case of 3 Hz where still the effect of actuation can be realized with a fuller velocity profile near the bottom wall.

Figure 12 displays time-averaged temperature profiles at various downstream stations for Re = 400. In the fully-developed flow region of the base flow, the temperature profile is linear as in the case Re = 200. Again, in the vicinity of the actuator (x/b = 4), frequencies 2 and 3 Hz trigger the most effective heat transfer inside the flow domain resulting in almost two-orders of magnitude increase in Nusselt number. Downstream near the exit of the channel (x/b = 30), the steepness of the temperature gradients reduce but still very large compared to the f = 0 and f = 1 Hz cases.

Figure 13(a) and (b) show the time-averaged Nusselt number distributions along the bottom and top walls of the channel flow Re = 400. It can be seen that the value of the Nusselt number for the base flow is around 2 in the fully developed region as Figure 4 indicates. With the JaVA-BFS activated at 2 and 3 Hz for instance, the time-averaged Nusselt number variations both along the bottom and top walls of the channel significantly increase and fluctuate in accordance with the vortical structures observed in Figs. 5 and 9. Note that in the vicinity of the JaVA-BFS, they peak as high as 100, two-orders of magnitude higher than the base flow. On the other hand, the influence of the actuation at 1 Hz is locally poor since we do not observe traveling vortical structures for this case. As expected, for all cases the Nu numbers decrease downstream of the channel since the influence of the JaVA-BFS actuation diminishes because of the viscous effects. Figure 14 indicates the overall-averaged Nusselt numbers along the bottom and top walls versus various jet-Reynolds numbers for Re = 400. With increasing jet-Reynolds number, the effectiveness of mixing through active flow control becomes more significant. The overall-averaged Nusselt number along the top wall remains almost the same for the non-actuating case and at Re_J = 100 but it jumps to much higher values at Re_J = 200 and 300. The overall-averaged Nusselt numbers along the bottom walls are higher than the overall-averaged Nusselt numbers along the top walls as a result of the more effective mixing of the JaVA-induced flows with the channel flow on the bottom. It should be mentioned that there is an almost linear increase between $0 < Re_J < 300$ in the overall-averaged Nusselt number along the bottom wall.

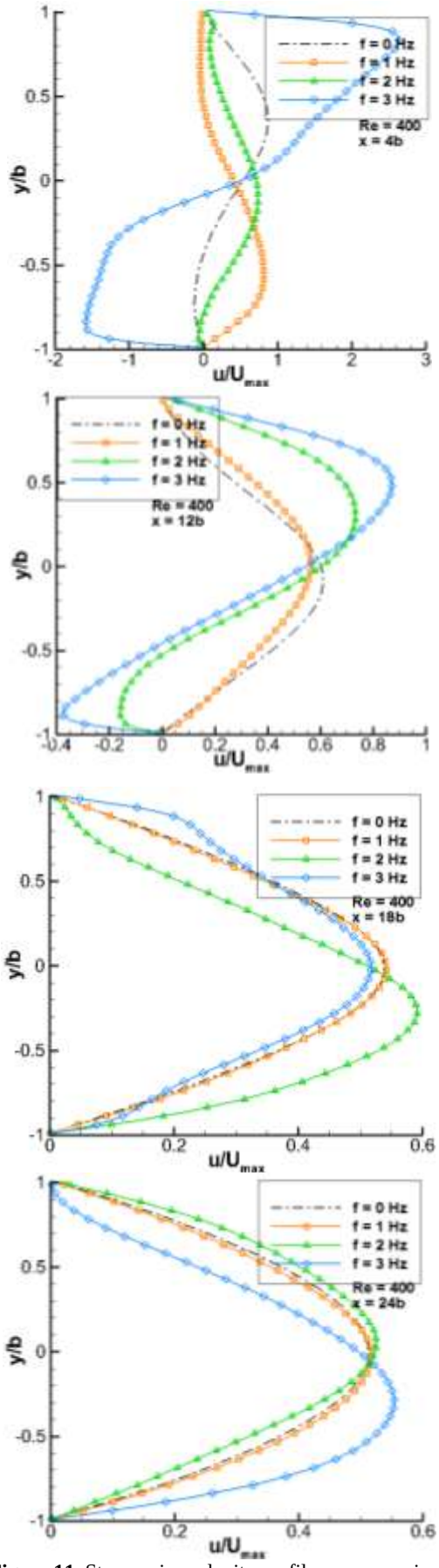

Figure 11. Streamwise velocity profiles across various channel locations, Re = 400.

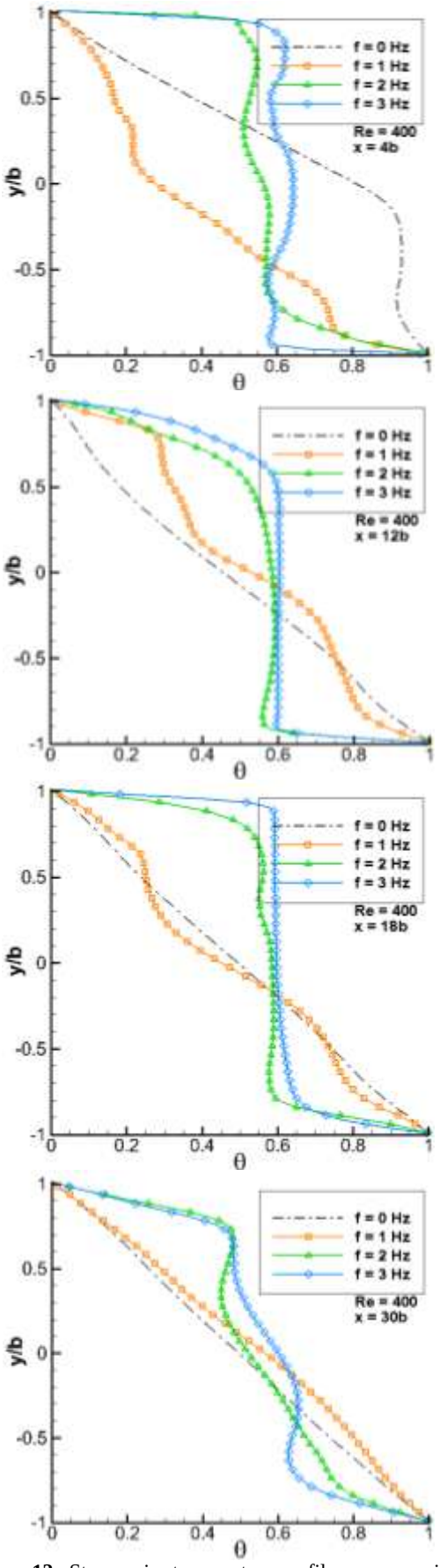

Figure 12. Streamwise temperature profiles across various channel locations, Re = 400.

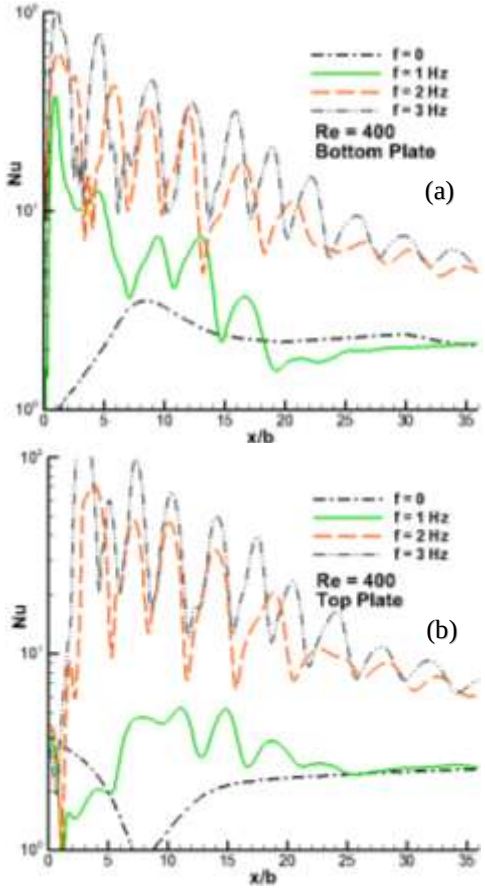

Figure 13. Time-averaged Nusselt number variation along the channel walls: (a) bottom plate (b) top plate for Re = 400.

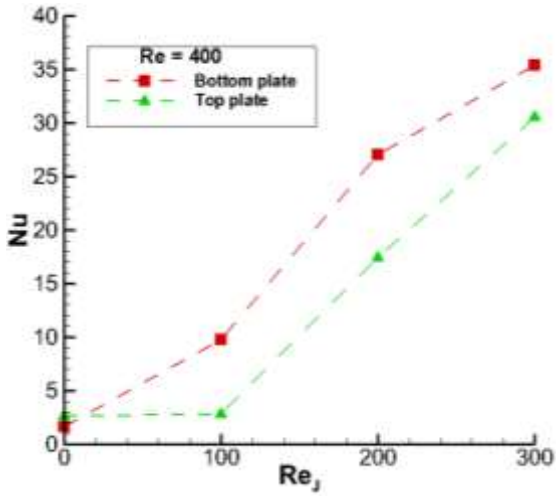

Figure 14. The variation of the overall-averaged Nusselt number as a function of the actuation frequency (or jet-Reynolds number) for the incoming flow Re = 400

CONCLUSIONS

In this study JaVA-BFS has been investigated numerically in a channel in an effort to increase the heat transfer. The ability of JaVA as a zero-net mass flux device to highly increase the rate of heat transfer is reported for various frequencies or jet-Reynolds numbers for the two incoming flow Reynolds numbers. It is shown that when JaVA-BFS is actuated strongly enough (here f = 2 Hz or more), locally two-orders of magnitude increase in Nu or, as a mean value an order of magnitude increase in Nu is achievable due to the very steep temperature gradients near the channel walls. It is reported that the JaVA-BFS induced vortical structures in the channel is the main mechanism for the very high increase of the heat transfer rate. It is also found that as the incoming flow Reynolds number increases, the extent of the traveling vortical structures moves far downstream distances and the Nu numbers are higher compared to the low values of incoming Reynolds number. This proposed JaVA-BFS induced active flow control approach is based on the suction and blowing of the recirculation zone of the common backward facing step and it is shown to be very effective for the flow mixing leading to a significant enhancement in the heat transfer.

ACKNOWLEDGEMENTS

We gratefully acknowledge the financial support of the Scientific and Technological Research Council of Turkey (TÜBİTAK) through the project "Development and Testing of a Jet and Vortex Actuator (JaVA) for Active Flow Control", Nr. 107M644.

REFERENCES

Alam, M.R., Liu, W. and Haller G., 2006, Closed loop separation control: an analytic approach, *Physics of Fluids*, 18, 043601.

Al-aswadi, A.A., Mohammed, H.A., Shuaib, N.H. and Campo, A., 2010, Laminar forced convection flow over a backward facing step using nanofluids, *International Communications in Heat and Mass Transfer*, 37, 950-957.

ANSYS-Fluent v.14, User's Manuel.

Cattafesta, L.N., 2009, Von Karman Institute (VKI)-Lecture Series, *Flow Control: fundamentals, advances and applications*. Brussels, Belgium.

Cadirci, S., Gunes, H., and Rist, U., 2010, Numerical Investigation of Jet and Vortex Actuator (JaVA) for Active Flow Control, *AIAA- 5th Flow Control* Conference, Chicago, 10.2514/6.2010-4410.

Cadirci, S., 2011, Experimental and numerical investigation of jet and vortex actuator for active flow control, Ph.D. Thesis, Institute of Science and Technology, Istanbul Technical University, Turkey.

Cadirci, S., Gunes, H., and Rist, U., 2012, Experimental Investigation of Jet and Vortex Actuator Using Particle Image Velocimetry, *ASME International Mechanical Engineering Congress & Exposition*, Houston, 10.1115/IMECE2012-86299.

Cadirci, S., Gunes, H., Rist, U., 2013, Active flow control applications with a jet and vortex actuator in a laminar cross flow, *International Journal of Heat and Fluid Flow*, 39, 146-159.

Creuse, E., Giovannini, A. and Mortazavi I., 2009, Vortex simulation of active control strategies for transitional backward facing step flows, *Computers and Fluids*, 38, 1348-1360.

Dandois, J., Garnier, E. and Sagaut, P., 2007, Numerical simulation of active separation control by a synthetic jet, *Journal of Fluid Mechanics*, 572, 25-58, Cambridge University Press.

Gunes, H., Cadirci, S., Baldani, F., Peters, B., and Rist, U., 2008, Temporal Analysis of Jet and Vortex Actuator (JaVA)-induced Flows, *International Conference on Jets, Wakes and Separated Flows*, ICJWSF, Berlin.

Johnston, J. P., and Nishi, M., 1990, Vortex Generator Jets-A Means for Separation Control, *AIAA Journal*, 28, No. 6, 989-994.

Lachowicz, J. T., Yao C., and Wlezien, R. W., 1999a, Physical Analysis and Scaling of a Jet and Vortex Actuator, *Proceedings of the 3rd ASME/JSME Joint Fluids Engineering Conference*, FEDSM'99-6921, ASME, San Francisco.

Lachowicz, J. T., Yao, C., and Wlezien, R. W., 1999b, Flow Field Characterization of a Jet and Vortex Actuator, *Experiments in Fluids*, 27, 12-20.

Nada, E.A., 2008, Application of nanofluids for heat transfer enhancement of separated flows encountered in a backward facing step, *International Journal of Heat and Fluid Flow*, 29, 2008, 242-249.

Seifert, A., and Pack, L., 1998, Oscillatory Control of Separation at High Reynolds Numbers, *36th Aerospace Sciences Meeting and Exhibit*, AIAA 98-0214, Reno, Nevada.

Uruba, V., Jonas, P. and Mazur O., 2007, Control of a channel flow behind a backward facing step by suction blowing, *International Journal of Heat and Fluid Flow*, 28, 665-672.